Front. Struct. Civ. Eng. 2015, 9(4): 341–358
DOI 10.1007/s11709-015-0302-1

RESEARCH ARTICLE

An extended cell-based smoothed discrete shear gap method (XCS-FEM-DSG3) for free vibration analysis of cracked Reissner-Mindlin shells

M. H. NGUYEN-THOI[a,b], L. Le-ANH[a,b], V. Ho-HUU[a,b], H. Dang-TRUNG[a,b], T. NGUYEN-THOI[a,b,*]

[a] *Division of Computational Mathematics and Engineering (CME), Institute for Computational Science (INCOS), Ton Duc Thang University, Hochiminh city, Vietnam*

[b] *Faculty of Civil Engineering, Ton Duc Thang University, Hochiminh city, Vietnam*

[*] *Corresponding author. E-mail: nguyenthoitrung@tdt.edu.vn*

ABSTRACT A cell-based smoothed discrete shear gap method (CS-FEM-DSG3) was recently proposed and proven to be robust for free vibration analyses of Reissner-Mindlin shell. The method improves significantly the accuracy of the solution due to softening effect of the cell-based strain smoothing technique. In addition, due to using only three-node triangular elements generated automatically, the CS-FEM-DSG3 can be applied flexibly for arbitrary complicated geometric domains. However so far, the CS-FEM-DSG3 has been only developed for analyzing intact structures without possessing internal cracks. The paper hence tries to extend the CS-FEM-DSG3 for free vibration analysis of cracked Reissner-Mindlin shells by integrating the original CS-FEM-DSG3 with discontinuous and crack – tip singular enrichment functions of the extended finite element method (XFEM) to give a so-called extended cell-based smoothed discrete shear gap method (XCS-FEM-DSG3). The accuracy and reliability of the novel XCS-FEM-DSG3 for free vibration analysis of cracked Reissner-Mindlin shells are investigated through solving three numerical examples and comparing with commercial software ANSYS.

KEYWORDS cracked Reissner-Mindlin shell, free vibration analysis, cell-based smoothed discrete shear gap method (CS-FEM-DSG3), extended cell-based smoothed discrete shear gap method (XCS-FEM-DSG3), smoothed finite element methods (SFEM)

1 Introduction

Shell structures are widely used in many engineering disciplines such as civil, mechanical, aerospace, marine engineering, etc. They can appear in various structures like shell roofs, pressure vessels, pipelines, tubular joints, offshore oil tanks, aircraft, submarines, etc. Similar to other types of structures, shell structures suffer from many types of defects in their service life owing to external agents such as corrosion, chemical attack, degradation, and so on. Among them, the appearance of cracks in shell structures is one of the most popular causes and makes reduce significantly their loading capacities. When a crack appears in shell structures, local flexibility and anisotropy arise right at the crack location. As a result, the characteristics of shell structures would significantly differ from those of intact shells. The simulation of the behavior of flawed shell structures thus becomes very important to evaluate the effects of these imperfections on loading capacity and safety in designing shell structures.

From the realistic demand of deep understanding cracked shell behaviors, many studies were conducted in the past decades. For example, in 1988, Kwon [1] developed a set of singular finite elements for application to problems of fracture mechanics in general. This set contained elements with derivative singularity between 0 and 1 which helps describe constant strain field and satisfy

Article history: Received Jan 28, 2015; Accepted May 2, 2015

the compatible condition along inter-element boundaries. Krawczuk et al. [2] analyzed the static deflections and natural frequencies of thin, rectangular shell structures with transverse, internal, open cracks. In this study, the crack was modeled by additional flexibility matrices calculated on the basic laws of fracture mechanics. Liu et al. [3] developed the formulation of crack shell based on the linearized shallow shell theory, by including the effect of the crack-face closure on the stress intensity factors. Vaziri et al. [4], in 2006, used linear eigenvalue analysis to formulate cracked cylindrical shells under combined internal pressure and axial compression. In this study, some insight into the effect of internal pressure on critical crack length was provided. Fu et al. [5], in 2012, proposed an approach based on the transverse or out-of-plane nonlinear dynamic response at the centers of crack edges in a cracked cylindrical shell structure. This approach helped avoid the problem of mesh selection at the crack tip in the finite element analysis for bulging factors and provided information about the influence of crack lengths as well as crack widths on responses. Among these proposed methods, eXtended Finite Element Method (X-FEM) proposed by Belytschko et al. [6–8] is shown as one of the most robust and effective numerical methods for analyzing the behaviors of cracked structures. In this methodology, the enriched approximation is constructed from the interaction of the crack geometry with the mesh. In association with the level set method (LSM), the XFEM allows the entire crack to be represented independently of the mesh, and thus remeshing is not necessary in process of modeling crack growth. Banchene et al. [9] applied this method to study the free flexural vibrations of cracked plates using 4-noded field consistent enriched element. Natarajan et al. [10] also applied XFEM for free vibration analysis for FGM plates and obtained some good results. Besides, the enriched and extended formulations related to XFEM have been also employed by various methods for fracture analysis of plates and shells such as meshfree methods [11–13], phantom node method [14], isogeometric analysis [15,16], finite element methods [17–20], etc. It can be seen from the literature that studies related to analysis of cracked shells using shear-locking-free triangular shell elements is somewhat limited. This paper hence will try to fill this gap by using a new three-node triangular shell element proposed recently for free vibration analysis of cracked Reissner-Mindlin shells.

In the other front of the development of numerical methods, Liu and Nguyen-Thoi et al. [21] have integrated the strain smoothing technique into the FEM to create a series of smoothed FEM (S-FEM) such as cell-based smoothed FEM (CS-FEM) [22–24], node-based smoothed FEM (NS-FEM) [25–27], edge-based smoothed FEM (ES-FEM) [28,29], face-based smoothed FEM (FS-FEM) [30] and a group of alpha-FEM [31–34]. Each of these smoothed FEM has different properties and has been used to produce desired solutions for a wide class of benchmark and practical mechanics problems. Several theoretical aspects of the S-FEM models have been provided in Refs. [35,36]. The S-FEM models have also been further investigated and applied to various problems such as plates and shells [37–50], piezoelectricity [51,52], fracture mechanics [53], visco-elastoplasticity [54–56], limit and shakedown [57,58], and some other applications [59,60], etc.

Among them, the cell-based smoothed discrete shear gap method CS-FEM-DSG3 [45], which is a combination of the CS-FEM and discrete shear gap method (DSG3) [61], is one of the most effective methods for static and free vibration analyses of Reissner-Mindlin shells. The CS-FEM-DSG3 is free of shear locking and achieves the high accuracy compared to the exact solutions and others existing elements in the literature. Besides such advantages, the implementation of the CS-FEM-DSG3 is also simple since it only uses the three-node triangular elements which can be easily generated automatically, especially for arbitrary complicated geometric domains. Due to these outstanding properties, the CS-FEM-DSG3 then has been extended to analyze various problems such as flat shells [45], stiffened plates [43], FGM plates [62], composite plates [63], piezoelectricity plates [51], and dynamic responses of plates on the viscoelastic foundation [64,65]. However so far, the CS-FEM-DSG3 has been only developed to analyze perfect structures without possessing internal cracks.

The paper hence extends the CS-FEM-DSG3 for free vibration analysis of cracked cylindrical shells by integrating itself with discontinuous and crack – tip singular enrichment functions of the XFEM to give a so-called extended cell-based smoothed discrete shear gap method (XCS-FEM-DSG3). In the formulation of XCS-FEM-DSG3 method, enrichment functions are used to model the discontinuities at crack locations. By using level-set method in the X-FEM, the finite element mesh can be discretized independently of the crack locations. The formulation of CS-FEM-DSG3 will be combined with the discontinuous enrichment functions and the singular functions of X-FEM to compute the stiffness matrices of elements cut by the crack. On the other hand, for un-cut elements, stiffness matrices are normally computed by the original CS-FEM-DSG3. The obtained results through three numerical examples are compared with those of commercial software ANSYS to illustrate the accuracy and robustness of the XCS-FEM-DSG3 in solving free vibration analysis of cracked cylindrical Reissner-Mindlin shells.

The paper is then organized as follows. Section 2 generally introduces the weakform of the Reissner-Mindlin shells. In Section 3, the formulation of XCS-FEM-DSG3 for cracked shells are presented. Section 4 performs numerical examples to verify the reliability and efficiency of the proposed method. Finally, some conclusions are withdrawn in Section 5.

2 Weakform of the Reissner – Mindlin shells

Shell structures are usually subjected to both membrane and bending forces. Hence, in this paper, the cylindrical shell is modeled by the flat shell element which is a combination of a membrane element and a bending plate element. In this flat shell element, the middle surface of shell is chosen as the reference plane that occupies a domain $\Omega \in \mathbb{R}^3$ as shown in Fig. 1.

Let u, v, w be the displacements of the middle plane in the x, y, z directions, and β_x, β_y, β_z be the rotations of the middle plane around y-axis, x-axis, and z-axis respectively. Then, the unknown vector of six independent field variables at any point in the Reissner – Mindlin shell domain is written as, $\mathbf{u} = \begin{bmatrix} u & v & w & \beta_x & \beta_y & \beta_z \end{bmatrix}^{\mathrm{T}}$, in local coordinate system $oxyz$.

According to the first-order shear deformation theory (FSDT), the membrane strain $\boldsymbol{\varepsilon}_m$, the bending strain $\boldsymbol{\kappa}$ and the shear strain $\boldsymbol{\gamma}$ are respectively defined as

$$\boldsymbol{\varepsilon}_m = \begin{bmatrix} u_{,x} \\ v_{,y} \\ u_{,y} + v_{,x} \end{bmatrix}; \boldsymbol{\kappa} = \begin{bmatrix} \beta_{x,x} \\ \beta_{y,y} \\ \beta_{x,y} + \beta_{y,x} \end{bmatrix}; \boldsymbol{\gamma} = \begin{bmatrix} \beta_x + w_{,x} \\ \beta_y + w_{,y} \end{bmatrix}, \tag{1}$$

where the subscript "comma" represents the partial derivative with respect to the spatial coordinate succeeding it.

Using the Hamilton principle, the general weakform of the Reissner – Mindlin shells for free vibration problems can be expressed as

$$\int_\Omega \begin{bmatrix} \delta(\boldsymbol{\varepsilon}_m)^{\mathrm{T}} & \delta(\boldsymbol{\kappa})^{\mathrm{T}} & \delta(\boldsymbol{\gamma})^{\mathrm{T}} \end{bmatrix} \begin{bmatrix} \mathbf{D}_m & 0 & 0 \\ 0 & \mathbf{D}_b & 0 \\ 0 & 0 & \mathbf{D}_s \end{bmatrix} \begin{bmatrix} \boldsymbol{\varepsilon}_m \\ \boldsymbol{\kappa} \\ \boldsymbol{\gamma} \end{bmatrix} \mathrm{d}\Omega + \int_\Omega \delta(\mathbf{u})^{\mathrm{T}} \mathbf{m} \mathbf{u} \mathrm{d}\Omega = 0, \tag{2}$$

where $\mathbf{D}_m$, $\mathbf{D}_b$ and $\mathbf{D}_s$ are the material matrices related to the membrane, the bending and the shear deformations, calculated respectively as

$$\mathbf{D}_m = \frac{Eh}{(1-\nu^2)} \begin{bmatrix} 1 & \nu & 0 \\ \nu & 1 & 0 \\ 0 & 0 & (1-\nu)/2 \end{bmatrix};$$

$$\mathbf{D}_b = \frac{Eh^3}{12(1-\nu^2)} \begin{bmatrix} 1 & \nu & 0 \\ \nu & 1 & 0 \\ 0 & 0 & (1-\nu)/2 \end{bmatrix};$$

$$\mathbf{D}_s = kh \begin{bmatrix} \mu & 0 \\ 0 & \mu \end{bmatrix}, \tag{3}$$

in which E, h, ν and μ are, respectively, Young's modulus, shell thickness, Poisson ratio and shear modulus; $k = 5/6$ is the shear correction factor; and $\mathbf{m}$ is the mass matrix containing the mass density of the material ρ and is expressed as

$$\mathbf{m} = \mathrm{diag}[\rho h, \rho h, \rho h, \rho h^3/12, \rho h^3/12, 0]. \tag{4}$$

3 Formulation of the extended cell-based smoothed discrete shear gap method (XCS-FEM-DSG3) for cracked cylindrical shells

3.1 A brief on the formulation of the CS-FEM-DSG3 for shell structures

For the formulation of shell structures, the flat shell element is formulated first in local coordinate system $oxyz$, then, it is transformed to the global coordinate system $OXYZ$. In the formulation of the CS-FEM-DSG3, each triangular element Ω_e is further divided into three sub-triangles Δ_1, Δ_2 and Δ_3 by connecting the central point O of the element to three field nodes as shown in Fig. 2. Then, in each sub-triangle, the stabilized DSG3 [61] is used to compute the strain field of shell. Finally the strain smoothing technique is applied on the whole triangular element to smooth the strains on these three sub-triangles.

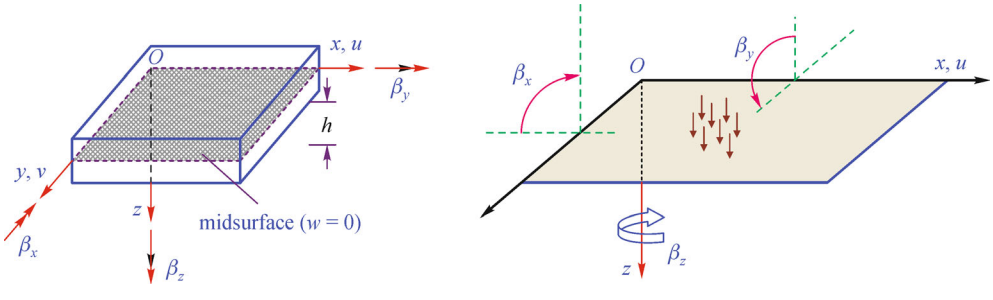

Fig. 1 Reissner–Mindlin flat shell and positive directions of displacements u, v, w and three rotations β_x, β_y and β_z

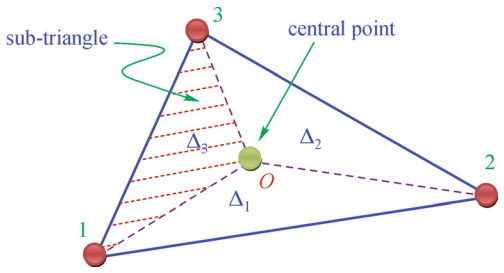

Fig. 2 Three sub-triangles (Δ_1, Δ_2 and Δ_3) created from the triangle 1-2-3 in the CS-FEM-DSG3 by connecting the central point O with three field nodes 1, 2 and 3

More details of the formulation of the CS-FEM-DSG3 can be found in [43,45,62,64].

In the CS-FEM-DSG3, the displacement vector $\mathbf{d}_O^e = [u_O^e \quad v_O^e \quad w_O^e \quad \beta_{xO}^e \quad \beta_{yO}^e \quad \beta_{zO}^e]^{\mathrm{T}}$ at the central point O of an element is assumed to be the simple average of three displacement vectors $\mathbf{d}_1^e$, $\mathbf{d}_2^e$, $\mathbf{d}_3^e$ of three field nodes, and has the form of

$$\mathbf{d}_O^e = \frac{1}{3}(\mathbf{d}_1^e + \mathbf{d}_2^e + \mathbf{d}_3^e). \tag{5}$$

On the first sub-triangle Δ_1 (triangle O-1-2), the linear approximation $\mathbf{u}^{e\Delta_1} = [u^{e\Delta_1} \quad v^{e\Delta_1} \quad w^{e\Delta_1} \quad \beta_x^{e\Delta_1} \quad \beta_y^{e\Delta_1} \quad \beta_z^{e\Delta_1}]^{\mathrm{T}}$ is constructed by

$$\mathbf{u}^{e\Delta_1} = N_1^{e\Delta_1}\mathbf{d}_O^e + N_2^{e\Delta_1}\mathbf{d}_1^e + N_3^{e\Delta_1}\mathbf{d}_2^e = \mathbf{N}^{e\Delta_1}\mathbf{d}^{e\Delta_1}, \tag{6}$$

where $\mathbf{d}^{e\Delta_1} = [\mathbf{d}_O^e \quad \mathbf{d}_1^e \quad \mathbf{d}_2^e]^{\mathrm{T}}$ is the vector of nodal degrees of freedom of the sub-triangle Δ_1 and $\mathbf{N}^{e\Delta_1} = [N_1^{e\Delta_1} \quad N_2^{e\Delta_1} \quad N_3^{e\Delta_1}]$ contains the linear shape functions created by the sub-triangle Δ_1 in natural coordinate defined by

$$N_1 = 1-\eta-\xi;\ N_2 = \xi;\ N_3 = \eta. \tag{7}$$

Using the DSG3 formulation [61] for the sub-triangle Δ_1, the membrane, bending and shear strains $\boldsymbol{\varepsilon}_m^{e\Delta_1}$, $\boldsymbol{\kappa}^{e\Delta_1}$ and $\boldsymbol{\gamma}^{e\Delta_1}$ in the sub-triangle Δ_1 are then obtained, respectively, by

$$\boldsymbol{\varepsilon}_m^{e\Delta_1} = \underbrace{\begin{bmatrix}\mathbf{b}_1^{m\Delta_1} & \mathbf{b}_2^{m\Delta_1} & \mathbf{b}_3^{m\Delta_1}\end{bmatrix}}_{\mathbf{b}^{m\Delta_1}} \begin{bmatrix}\mathbf{d}_O^e \\ \mathbf{d}_1^e \\ \mathbf{d}_2^e\end{bmatrix} = \mathbf{b}^{m\Delta_1}\mathbf{d}^{e\Delta_1}, \tag{8}$$

$$\boldsymbol{\kappa}^{e\Delta_1} = \underbrace{\begin{bmatrix}\mathbf{b}_1^{b\Delta_1} & \mathbf{b}_2^{b\Delta_1} & \mathbf{b}_3^{b\Delta_1}\end{bmatrix}}_{\mathbf{b}^{b\Delta_1}} \begin{bmatrix}\mathbf{d}_O^e \\ \mathbf{d}_1^e \\ \mathbf{d}_2^e\end{bmatrix} = \mathbf{b}^{b\Delta_1}\mathbf{d}^{e\Delta_1}, \tag{9}$$

$$\boldsymbol{\gamma}^{e\Delta_1} = \underbrace{\begin{bmatrix}\mathbf{b}_1^{s\Delta_1} & \mathbf{b}_2^{s\Delta_1} & \mathbf{b}_3^{s\Delta_1}\end{bmatrix}}_{\mathbf{b}^{s\Delta_1}} \begin{bmatrix}\mathbf{d}_O^e \\ \mathbf{d}_1^e \\ \mathbf{d}_2^e\end{bmatrix} = \mathbf{b}^{s\Delta_1}\mathbf{d}^{e\Delta_1}, \tag{10}$$

where $\mathbf{b}^{m\Delta_1}$, $\mathbf{b}^{b\Delta_1}$ and $\mathbf{b}^{s\Delta_1}$ are the matrices of shape function derivatives related to membrane, bending and shear deformation of the triangular elements, calculated as

$$\mathbf{b}^{m\Delta_1} = \begin{bmatrix} b-c & 0 & 0 & 0 & 0 & 0 & c & 0 & 0 & 0 & 0 & 0 & -b & 0 & 0 & 0 & 0 & 0 \\ 0 & d-a & 0 & 0 & 0 & 0 & 0 & -d & 0 & 0 & 0 & 0 & 0 & a & 0 & 0 & 0 & 0 \\ d-a & b-c & 0 & 0 & 0 & 0 & -d & c & 0 & 0 & 0 & 0 & a & -b & 0 & 0 & 0 & 0 \end{bmatrix}, \tag{11}$$

$$\mathbf{b}^{b\Delta_1} = \begin{bmatrix} 0 & 0 & 0 & b-c & 0 & 0 & 0 & 0 & 0 & c & 0 & 0 & 0 & 0 & 0 & -b & 0 & 0 \\ 0 & 0 & 0 & 0 & d-a & 0 & 0 & 0 & 0 & 0 & -d & 0 & 0 & 0 & 0 & 0 & a & 0 \\ 0 & 0 & 0 & d-a & b-c & 0 & 0 & 0 & 0 & -d & c & 0 & 0 & 0 & 0 & a & -b & 0 \end{bmatrix}, \tag{12}$$

$$\mathbf{b}^{s\Delta_1} = \frac{1}{2A_e}\begin{bmatrix} 0 & 0 & b-c & A_e & 0 & 0 & 0 & 0 & c & ac/2 & bc/2 & 0 & 0 & 0 & -b & -bd/2 & -bc/2 & 0 \\ 0 & 0 & d-a & 0 & A_e & 0 & 0 & 0 & -d & -ad/2 & -bd/2 & 0 & 0 & 0 & a & ad/2 & ac/2 & 0 \end{bmatrix}, \tag{13}$$

with $a = x_2 - x_1$; $b = y_2 - y_1$; $c = y_3 - y_1$; $d = x_3 - x_1$ where $\mathbf{x}_i = [x_i \quad y_i]^{\mathrm{T}}$, $i = 1,2,3$ are coordinates of three nodes in the local coordinate system and A_e is the area of the triangular element as shown in Fig. 3.

Substituting $\mathbf{d}_O^e$ in Eq. (5) into Eqs. (8–10), and then rearranging, we obtain

$$\boldsymbol{\varepsilon}_m^{e\Delta_1} = \underbrace{\begin{bmatrix}\frac{1}{3}\mathbf{b}_1^{m\Delta_1} + \mathbf{b}_2^{m\Delta_1} & \frac{1}{3}\mathbf{b}_1^{m\Delta_1} + \mathbf{b}_3^{m\Delta_1} & \frac{1}{3}\mathbf{b}_1^{m\Delta_1}\end{bmatrix}}_{\mathbf{B}^{m\Delta_1}} \begin{bmatrix}\mathbf{d}_1^e \\ \mathbf{d}_2^e \\ \mathbf{d}_3^e\end{bmatrix} = \mathbf{B}^{m\Delta_1}\mathbf{d}^e, \tag{14}$$

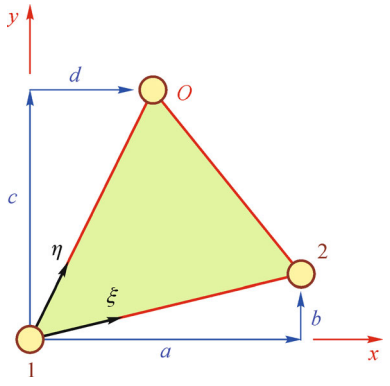

Fig. 3 Three-node triangular element and local coordinates in the conventional DSG3

$$\boldsymbol{\kappa}^{e\Delta_1} = \underbrace{\begin{bmatrix} \frac{1}{3}\mathbf{b}_1^{b\Delta_1} + \mathbf{b}_2^{b\Delta_1} & \frac{1}{3}\mathbf{b}_1^{b\Delta_1} + \mathbf{b}_3^{b\Delta_1} & \frac{1}{3}\mathbf{b}_1^{b\Delta_1} \end{bmatrix}}_{\mathbf{B}^{b\Delta_1}} \begin{bmatrix} \mathbf{d}_1^e \\ \mathbf{d}_2^e \\ \mathbf{d}_3^e \end{bmatrix} = \mathbf{B}^{b\Delta_1}\mathbf{d}^e, \tag{15}$$

$$\boldsymbol{\gamma}^{e\Delta_1} = \underbrace{\begin{bmatrix} \frac{1}{3}\mathbf{b}_1^{s\Delta_1} + \mathbf{b}_2^{s\Delta_1} & \frac{1}{3}\mathbf{b}_1^{s\Delta_1} + \mathbf{b}_3^{s\Delta_1} & \frac{1}{3}\mathbf{b}_1^{s\Delta_1} \end{bmatrix}}_{\mathbf{B}^{s\Delta_1}} \begin{bmatrix} \mathbf{d}_1^e \\ \mathbf{d}_2^e \\ \mathbf{d}_3^e \end{bmatrix} = \mathbf{B}^{s\Delta_1}\mathbf{d}^e. \tag{16}$$

Similarly, by using cyclic permutation, we easily obtain the membrane, bending and shear strains $\boldsymbol{\varepsilon}_m^{e\Delta_j}$, $\boldsymbol{\kappa}^{e\Delta_j}$, $\boldsymbol{\gamma}^{e\Delta_j}$ and matrices $\mathbf{B}^{m\Delta_j}$, $\mathbf{B}^{b\Delta_j}$, $\mathbf{B}^{s\Delta_j}$, $j = 2,3$, for the second sub-triangle Δ_2 (triangle O-2-3) and third sub-triangle Δ_3 (triangle O-3-1), respectively. Then, the strain smoothing technique is applied on the whole triangular element to smooth the strains. The elemental smoothed strains $\tilde{\boldsymbol{\varepsilon}}_m^e$, $\tilde{\boldsymbol{\kappa}}^e$ and $\tilde{\boldsymbol{\gamma}}^e$ are then expressed by

$$\tilde{\boldsymbol{\varepsilon}}_m^e = \tilde{\mathbf{B}}_m^e\mathbf{d}^e;\ \tilde{\boldsymbol{\kappa}}^e = \tilde{\mathbf{B}}_b^e\mathbf{d}^e;\ \tilde{\boldsymbol{\gamma}}^e = \tilde{\mathbf{B}}_s^e\mathbf{d}^e, \tag{17}$$

where $\tilde{\mathbf{B}}_m^e$, $\tilde{\mathbf{B}}_b^e$, $\tilde{\mathbf{B}}_s^e$ are the smoothed strain gradient matrices, respectively, given by

$$\tilde{\mathbf{B}}_i^e = \sum_{j=1}^{3}\int_{\Delta_j} \mathbf{B}_i^{\Delta_j}\Phi_e(\mathbf{x})\mathrm{d}\Omega;\ i = m,b,s;\ j = 1,2,3, \tag{18}$$

in which $\Phi_e(\mathbf{x})$ is a smoothing function presented as

$$\Phi_e(\mathbf{x}) = \begin{cases} 1/A_e & \mathbf{x} \in \Omega_e \\ 0 & \mathbf{x} \notin \Omega_e \end{cases}, \tag{19}$$

with A^e is the area of the whole triangular element; $\mathbf{B}_i^{\Delta_j}$ is the strain gradient matrix with respect to the sub-triangular element Δ_j.

By substituting Eq. (17) to the general weakform of the Reissner–Mindlin shells in Eq. (2), the governing equation for free vibration analysis becomes

$$(\mathbf{K} - \omega^2\mathbf{M})\mathbf{d} = \mathbf{0}, \tag{20}$$

where ω is the natural frequency; $\mathbf{d}$ is the nodal unknown vector of variables; $\mathbf{M}$ and $\mathbf{K}$ are the global mass and stiffness matrices computed by assembling the elemental mass and stiffness matrices as

$$\mathbf{M}^e = \mathbf{T}^T\left(\int_{\Omega_e}(\mathbf{N})^T\mathbf{m}\mathbf{N}\mathrm{d}\Omega\right)\mathbf{T}, \tag{21}$$

$$\mathbf{K}^e = \mathbf{T}^T\left(\int_{\Omega_e}\tilde{\mathbf{B}}_m^{eT}\mathbf{D}_m\tilde{\mathbf{B}}_m^e\mathrm{d}\Omega + \int_{\Omega_e}\tilde{\mathbf{B}}_b^{eT}\mathbf{D}_b\tilde{\mathbf{B}}_b^e\mathrm{d}\Omega + \int_{\Omega_e}\tilde{\mathbf{B}}_s^{eT}\mathbf{D}_s\tilde{\mathbf{B}}_s^e\mathrm{d}\Omega\right)\mathbf{T}, \tag{22}$$

where $\mathbf{T}$ is the transformation matrix of coordinates from the local coordinate system $oxyz$ to the global coordinate system $OXYZ$ as shown in Fig. 4.

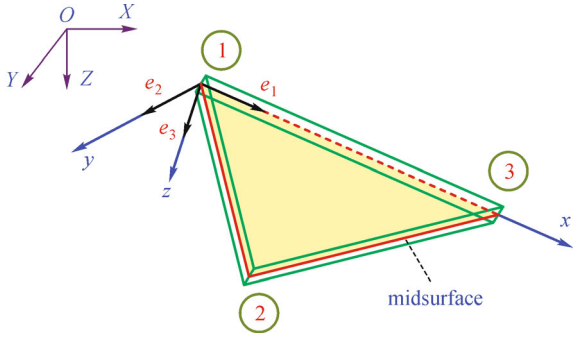

Fig. 4 Coordinate transformation in the triangular flat shell elements

It was suggested [66] that a stabilization term should be added to improve the accuracy of approximate solution and to stabilize shear force oscillations. In this modification, $\mathbf{D}_s$ in Eq. (22) is replaced by $\hat{\mathbf{D}}_s$ as

$$\hat{\mathbf{D}}_s = \frac{kh^3}{h^2 + \alpha h_e^2}\begin{bmatrix} 1 & 0 \\ 0 & 1 \end{bmatrix}, \tag{23}$$

in which h_e is the longest length of the element and α is a positive constant [67].

From Eqs. (11) – (17) and (22), it can be seen that the values of stiffness matrix at the drilling degree of freedom β_z is equal to zero. This causes the singularity to the global stiffness matrix when all elements meeting at a node are coplanar. To overcome this problem, these null value in the stiffness corresponding to the drilling degree of freedom

are replaced by approximate values which equal to 10^{-3} times the maximum diagonal value in the element stiffness matrix [60]. It also can be observed that the element stiffness matrix in the CS-FEM-DSG3 is no longer depend on the sequence of nodes in elements as in the conventional DSG3. This helps improve accuracy as well as the stability of the DSG3, especially for the coarse or distorted meshes.

3.2 A brief on extended finite element method (X-FEM) and its integration to CS-FEM-DSG3

Based on the idea of partition unity of Babuška et al. [68], Belytschko and Black [6] proposed the extended finite element method (X-FEM) for solving linear elastic fracture mechanic problems. The key point of the X-FEM is adding discontinuous and singular enrichment functions besides conventional expansion of the displacement field in order to capture the effects of cracks or other local discontinuities within the mesh. In the XFEM, the mesh is first generated normally without considering the presence of cracks or discontinuities. This helps overcome the difficulties of remeshing as in conventional FEM when solving problems related to crack, especially crack propagation. Then, the cracks or other discontinuities are modeled by the generalized Heaviside function and singularly asymptotic functions. This section will present a brief overview of the X-FEM for shells. Further formulation can be found at [6,69–72] for interested readers.

In general, the field variables are approximated by

$$\mathbf{u}^h(\mathbf{x}) = \sum_{i \in N^{\mathrm{FEM}}} \mathbf{N}_i(\mathbf{x})\mathbf{d}_i + \text{enrichment parts}, \tag{24}$$

where $\mathbf{N}_i(\mathbf{x})$ are standard finite element shape functions; $\mathbf{d}_i$ are nodal variables associated with i^{th} node; N^{FEM} is the number of nodes in the whole mesh.

For cracked shells, the finite element approximation of shell displacements and section rotations is expressed in the form [73] of

$$\begin{aligned}(u^h,v^h,w^h)(\mathbf{x}) = &\underbrace{\sum_{i \in N^{\mathrm{FEM}}} N_i(\mathbf{x})(u_i,v_i,w_i)}_{u^h,v^h,w^h_{.\mathrm{cont}}} \\ &+ \underbrace{\sum_{j \in N^{\mathrm{H}}} N_j(\mathbf{x})H(\mathbf{x})(b_j^u,b_j^v,b_j^w)}_{u^h,v^h,w^h_{.\mathrm{split}}} \\ &+ \underbrace{\sum_{k \in N^B} N_k(\mathbf{x})\left(\sum_{l=1}^{4} G_l(r,\theta)(c_{kl}^u,c_{kl}^v,c_{kl}^w)\right)}_{u^h,v^h,w^h_{.\mathrm{tip}}},\end{aligned} \tag{25}$$

$$\begin{aligned}(\beta_x^h,\beta_y^h,\beta_z^h)(\mathbf{x}) = &\underbrace{\sum_{i \in N^{\mathrm{FEM}}} N_i(\mathbf{x})(\beta_{xi},\beta_{yi},\beta_{zi})}_{\beta_x^h,\beta_y^h,\beta^h_{z.\mathrm{cont}}} \\ &+ \underbrace{\sum_{j \in N^{\mathrm{H}}} N_j(\mathbf{x})H(\mathbf{x})(b_j^{\beta_x},b_j^{\beta_y},b_j^{\beta_z})}_{\beta_x^h,\beta_y^h,\beta^h_{z.\mathrm{split}}} \\ &+ \underbrace{\sum_{k \in N^B} N_k(\mathbf{x})\left(\sum_{l=1}^{4} F_l(r,\theta)(c_{kl}^{\beta_x},c_{kl}^{\beta_y},c_{kl}^{\beta_z})\right)}_{\beta_x^h,\beta_y^h,\beta^h_{z.\mathrm{tip}}}.\end{aligned} \tag{26}$$

In Eqs. (25) and (26), $\mathbf{u}_{\mathrm{cont}} = \begin{bmatrix} u^h_{.\mathrm{cont}} & v^h_{.\mathrm{cont}} & w^h_{.\mathrm{cont}} & \beta^h_{x.\mathrm{cont}} & \beta^h_{y.\mathrm{cont}} & \beta^h_{z.\mathrm{cont}} \end{bmatrix}^{\mathrm{T}}$ is the continuous displacement and rotation fields; $\mathbf{u}_{\mathrm{split}} = \begin{bmatrix} u^h_{.\mathrm{split}} & v^h_{.\mathrm{split}} & w^h_{.\mathrm{split}} & \beta^h_{x.\mathrm{split}} & \beta^h_{y.\mathrm{split}} & \beta^h_{z.\mathrm{split}} \end{bmatrix}^{\mathrm{T}}$ is the displacement and rotation field of elements split by cracks; $\mathbf{u}_{\mathrm{tip}} = \begin{bmatrix} u^h_{.\mathrm{tip}} & v^h_{.\mathrm{tip}} & w^h_{.\mathrm{tip}} & \beta^h_{x.\mathrm{tip}} & \beta^h_{y.\mathrm{tip}} & \beta^h_{z.\mathrm{tip}} \end{bmatrix}^{\mathrm{T}}$ is displacement and rotation field of elements containing crack tips. N^{FEM}, N^H, N^B are, respectively, the total number of nodes of the mesh, number of enriched nodes whose support is split by cracks and number of enriched nodes whose support contains crack tips as shown in Fig. 5; $\mathbf{d}_i = \begin{bmatrix} u_i & v_i & w_i & \beta_{xi} & \beta_{yi} & \beta_{zi} \end{bmatrix}^{\mathrm{T}}$ is the nodal unknown vector associated with the continuous part of the finite solution, $\mathbf{b}_j = \begin{bmatrix} b_j^u & b_j^v & b_j^w & b_j^{\beta_x} & b_j^{\beta_y} & b_j^{\beta_z} \end{bmatrix}^{\mathrm{T}}$ is the nodal enriched degree of freedom vector related to Heaviside function $H(\mathbf{x})$, and $\mathbf{c}_{kl} = \begin{bmatrix} c_{kl}^u & c_{kl}^v & c_{kl}^w & c_{kl}^{\beta_x} & c_{kl}^{\beta_y} & c_{kl}^{\beta_z} \end{bmatrix}^{\mathrm{T}}$ is the nodal enriched degree of freedom vector associated with the elastic asymptotic crack-tip functions $F_l(r,\theta)$ or $G_l(r,\theta)$.

The first term of enrichment involves a Heaviside jump function $H(\mathbf{x})$ whose value is $+1$ above the crack and -1 below the crack and can be expressed as

$$H(\mathbf{x}) = \begin{cases} +1, & \text{if } (\mathbf{x}-\mathbf{x}^*)\cdot\mathbf{n} \geqslant 0; \\ -1, & \text{otherwise}, \end{cases} \tag{27}$$

where $\mathbf{x}$ is a sample (or Gauss) point; $\mathbf{x}^*$ (lies on the crack) is the closest point to $\mathbf{x}$; and $\mathbf{n}$ is the unit outward normal to the crack at $\mathbf{x}^*$ as shown in Fig. 6.

The second additional part of the enriched displacement field involves set of branch functions G_l, F_l to model the asymptotic features of the displacement field at the crack tip and defined by

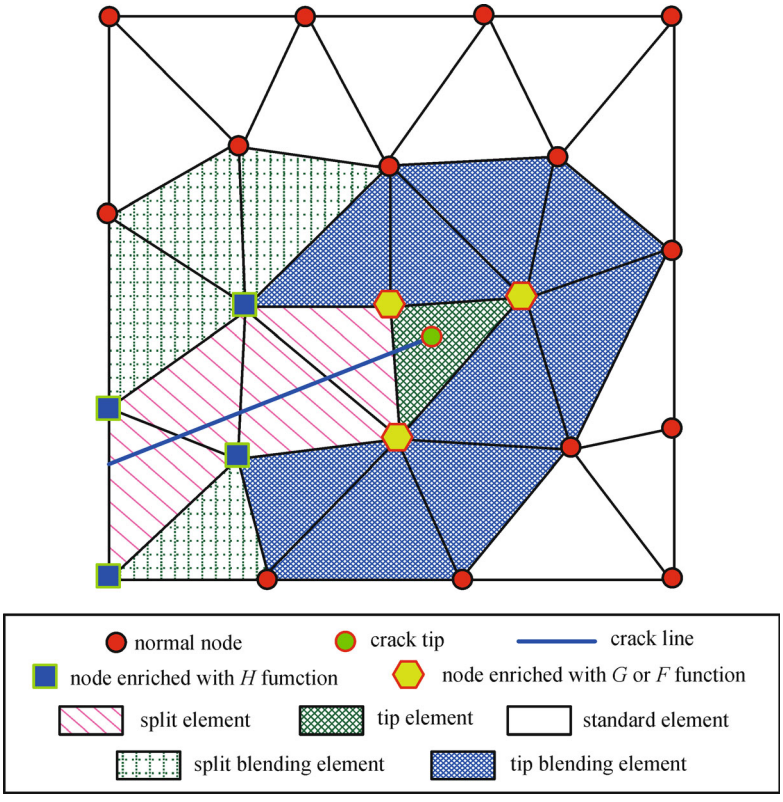

Fig. 5 Various kinds of elements and nodes in the XCS-FEM-DSG3

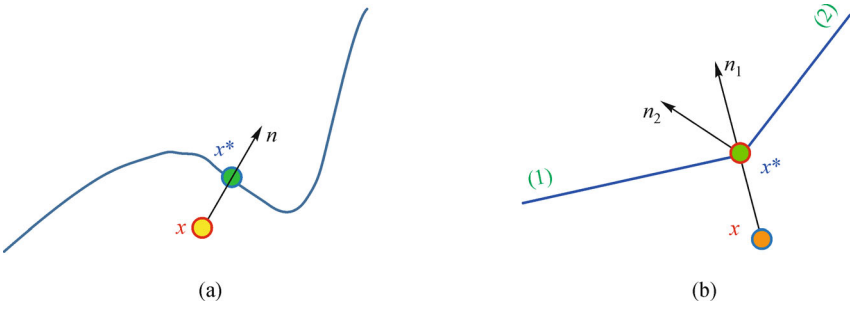

Fig. 6 Illustration of the unit outward normal to the crack at **x***: (a) a smoothed crack; (b) a crack with a kink

$$G_l(r,\theta)|_{l=1}^{4} \equiv \left\{r^{3/2}\sin\frac{\theta}{2}, r^{3/2}\cos\frac{\theta}{2}, r^{3/2}\sin\frac{3\theta}{2}, r^{3/2}\cos\frac{3\theta}{2}\right\}$$

$$F_l(r,\theta)|_{l=1}^{4} \equiv \left\{r\sin\frac{\theta}{2}, r\cos\frac{\theta}{2}, r\sin\frac{\theta}{2}\sin\theta, r\cos\frac{\theta}{2}\sin\theta\right\}, \quad (28)$$

where (r,θ) are polar coordinates in the local coordinate system with the origin at the crack tip.

When these enrichment functions are implemented to the CS-FEM-DSG3, the governing equation for free vibration of cracked shell now becomes

$$(\mathbf{K}-\omega^2\mathbf{M})\mathbf{e} = \mathbf{0}, \quad (29)$$

where ω is the natural frequency; $\mathbf{e} = \begin{bmatrix}\mathbf{d} & \mathbf{b}_j & \mathbf{c}_{kl}\end{bmatrix}$ is the nodal unknown vector of variables (for both classical and enriched ones). $\mathbf{M}$ and $\mathbf{K}$ are the global mass, stiffness matrices computed by assembling the element mass and stiffness matrices. For standard elements (unenriched elements), these $\mathbf{M}^e$ and $\mathbf{K}^e$ are normally calculated using the CS-FEM-DSG3 as stated in Section 3.1. For elements associated with cracks (enriched elements), these matrices are defined by follows. Note that in the following

equations, superscript *d, b, c* are respectively present for matrices related to un-enriched nodal degree of freedom, nodal degree of freedom enriched by Heaviside function b_j and nodal degree of freedom enriched by elastic asymptotic crack-tip functions c_{kl}.

$$\mathbf{M}^e = \begin{bmatrix} \mathbf{M}^{dd} & \mathbf{M}^{db} & \mathbf{M}^{dc} \\ \mathbf{M}^{bd} & \mathbf{M}^{bb} & \mathbf{M}^{bc} \\ \mathbf{M}^{cd} & \mathbf{M}^{cb} & \mathbf{M}^{cc} \end{bmatrix};$$
$$\mathbf{K}^e = \begin{bmatrix} \mathbf{K}^{dd} & \mathbf{K}^{db} & \mathbf{K}^{dc} \\ \mathbf{K}^{dc} & \mathbf{K}^{bb} & \mathbf{K}^{bc} \\ \mathbf{K}^{cd} & \mathbf{K}^{cb} & \mathbf{K}^{cc} \end{bmatrix}, \tag{30}$$

in which

$$\mathbf{M}^{rs} = \int_{\Omega_e} (\mathbf{N}^r)^T \mathbf{m}\, \mathbf{N}^s h \mathrm{d}\Omega \ (r,s = d,b,c), \tag{31}$$

$$\mathbf{K}^{rs} = \int_{\Omega_e} \left(\tilde{\mathbf{B}}_m^r\right)^T \mathbf{D}_m \tilde{\mathbf{B}}_m^s \mathrm{d}\Omega + \int_{\Omega_e} \left(\tilde{\mathbf{B}}_b^r\right)^T \mathbf{D}_b \tilde{\mathbf{B}}_b^s \mathrm{d}\Omega + \int_{\Omega_e} \left(\tilde{\mathbf{S}}^r\right)^T \mathbf{D}_s \tilde{\mathbf{S}}^s \mathrm{d}\Omega (r,s = d,b,c), \tag{32}$$

where Ω_e indicates the domain of the element; $\mathbf{N}^{r,s}$ are the matrices of shape functions given by

$$\mathbf{N}^d = [\mathbf{N}_1 \quad \mathbf{N}_2 \quad \mathbf{N}_3]; \mathbf{N}^b = [\mathbf{N}_1 H \quad \mathbf{N}_2 H \quad \mathbf{N}_3 H];$$
$$\mathbf{N}^c = \left[\mathbf{N}^{c1} \quad \mathbf{N}^{c2} \quad \mathbf{N}^{c3} \quad \mathbf{N}^{c4}\right]$$
$$\text{where } \mathbf{N}^{c\alpha} = [\mathbf{N}_1 F_\alpha \quad \mathbf{N}_2 F_\alpha \quad \mathbf{N}_3 F_\alpha]; \alpha = 1 \div 4. \tag{33}$$

$\tilde{\mathbf{B}}_m^r, \tilde{\mathbf{B}}_m^r, \tilde{\mathbf{S}}^r, r = d,b,c$, are the matrices of shape function derivatives related to membrane, bending and shear deformation calculated as followings. Note that in these equations, the notation $\mathbf{A} \circ \mathbf{B}$ represents Hadamard product of the two matrices $\mathbf{A}$ and $\mathbf{B}$.

$$\mathbf{B}_m^d = \tilde{\mathbf{B}}_m^e; \mathbf{B}_m^b = \mathbf{H} \circ \tilde{\mathbf{B}}_m^e;$$
$$\mathbf{B}_m^c = \left[\mathbf{F}_1 \circ \tilde{\mathbf{B}}_m^e \quad \mathbf{F}_2 \circ \tilde{\mathbf{B}}_m^e \quad \mathbf{F}_3 \circ \tilde{\mathbf{B}}_m^e \quad \mathbf{F}_4 \circ \tilde{\mathbf{B}}_m^e\right], \tag{34}$$

$$\mathbf{B}_b^d = \tilde{\mathbf{B}}_b^e; \mathbf{B}_b^b = \mathbf{H} \circ \tilde{\mathbf{B}}_b^e;$$
$$\mathbf{B}_b^c = \left[\mathbf{F}_1 \circ \tilde{\mathbf{B}}_b^e \quad \mathbf{F}_2 \circ \tilde{\mathbf{B}}_b^e \quad \mathbf{F}_3 \circ \tilde{\mathbf{B}}_b^e \quad \mathbf{F}_4 \circ \tilde{\mathbf{B}}_b^e\right], \tag{35}$$

$$\mathbf{S}^d = \tilde{\mathbf{B}}_s^e; \mathbf{S}^b = \mathbf{S} \circ \tilde{\mathbf{B}}_s^e;$$
$$\mathbf{S}^c = \left[\mathbf{G}_1 \circ \tilde{\mathbf{B}}_s^e \quad \mathbf{G}_2 \circ \tilde{\mathbf{B}}_s^e \quad \mathbf{G}_3 \circ \tilde{\mathbf{B}}_s^e \quad \mathbf{G}_4 \circ \tilde{\mathbf{B}}_s^e\right], \tag{36}$$

where $\boldsymbol{H}$, $\boldsymbol{F}_\alpha$, $\boldsymbol{S}$, $\boldsymbol{G}_\alpha$; $\alpha = 1 \div 4$ are matrices containing partial derivative of enrichment functions which is defined as follow:

$$\mathbf{H} = \begin{bmatrix} H_{,x} & 0 & 0 & H_{,x} & 0 & 0 & H_{,x} & 0 & 0 & H_{,x} & 0 & 0 & H_{,x} & 0 & 0 & H_{,x} & 0 & 0 \\ 0 & H_{,y} & 0 & 0 & H_{,y} & 0 & 0 & H_{,y} & 0 & 0 & H_{,y} & 0 & 0 & H_{,y} & 0 & 0 & H_{,y} & 0 \\ H_{,y} & H_{,x} & 0 & H_{,y} & H_{,x} & 0 & H_{,y} & H_{,x} & 0 & H_{,y} & H_{,x} & 0 & H_{,y} & H_{,x} & 0 & H_{,y} & H_{,x} & 0 \end{bmatrix}, \tag{37}$$

$$\mathbf{F}_\alpha = \begin{bmatrix} F_{\alpha,x} & 0 & 0 & F_{\alpha,x} & 0 & 0 & F_{\alpha,x} & 0 & 0 & F_{\alpha,x} & 0 & 0 & F_{\alpha,x} & 0 & 0 & F_{\alpha,x} & 0 & 0 \\ 0 & F_{\alpha,y} & 0 & 0 & F_{\alpha,y} & 0 & 0 & F_{\alpha,y} & 0 & 0 & F_{\alpha,y} & 0 & 0 & F_{\alpha,y} & 0 & 0 & F_{\alpha,y} & 0 \\ F_{\alpha,y} & F_{\alpha,x} & 0 & F_{\alpha,y} & F_{\alpha,x} & 0 & F_{\alpha,y} & F_{\alpha,x} & 0 & F_{\alpha,y} & F_{\alpha,x} & 0 & F_{\alpha,y} & F_{\alpha,x} & 0 & F_{\alpha,y} & F_{\alpha,x} & 0 \end{bmatrix}, \tag{38}$$

$$\mathbf{S} = \begin{bmatrix} 0 & 0 & H_{,x} & H & 0 & 0 & 0 & 0 & H_{,x} & H & 0 & 0 & 0 & 0 & H_{,x} & H & 0 & 0 \\ 0 & 0 & H_{,y} & 0 & H & 0 & 0 & 0 & H_{,y} & 0 & H & 0 & 0 & 0 & H_{,y} & 0 & H & 0 \end{bmatrix}, \tag{39}$$

$$\mathbf{G}_\alpha = \begin{bmatrix} 0 & 0 & G_{\alpha,x} & F_\alpha & 0 & 0 & 0 & 0 & G_{\alpha,x} & F_\alpha & 0 & 0 & 0 & 0 & G_{\alpha,x} & F_\alpha & 0 & 0 \\ 0 & 0 & G_{\alpha,y} & 0 & F_\alpha & 0 & 0 & 0 & G_{\alpha,y} & 0 & F_\alpha & 0 & 0 & 0 & G_{\alpha,y} & 0 & F_\alpha & 0 \end{bmatrix}, \tag{40}$$

in which $\tilde{\mathbf{B}}_m^e$, $\tilde{\mathbf{B}}_b^e$ and $\tilde{\mathbf{B}}_s^e$ are strain gradient matrices related to membrane, bending and shear deformation of triangular element which are calculated as Eq. (18).

3.3 Methodology of the coupling XCS-FEM-DSG3

As presented above, the CS-FEM-DSG3 is extended for

free vibration analysis of cracked FGM shells by integrating the CS-FEM-DSG3 itself with discontinuous and crack – tip singular enrichment functions of the X-FEM. This novel element is hence called the extended cell-based smoothed discrete shear gap shell element (XCS-FEM-DSG3).

In summary of the formulation of XCS-FEM-DSG3 for cracked shell, first, the mesh is generated independently of cracks location. After that, the formulation of CS-FEM-DSG3 is used to calculate strain gradient matrices $\tilde{\mathbf{B}}_m$, $\tilde{\mathbf{B}}_b$, $\tilde{\mathbf{B}}_s$ of all elements without any notion about cracks as in Eq. (18). Then, these matrices are enriched with discontinuous Heaviside function or elastic asymptotic crack-tip functions appropriately as in Eqs. (34)–(36) to calculate $\tilde{\mathbf{B}}_m^r$, $\tilde{\mathbf{B}}_m^r$, $\tilde{\mathbf{S}}^r$; $r = d,b,c$. The global mass, force and stiffness matrices $\mathbf{M}$, $\mathbf{K}$ are then computed using Eqs. (30)–(32).

In numerical implementation of XCS-FEM-DSG3, these strain gradient and global matrices are computed at the Gauss points using numerical Gauss quadrature. As a result, it is necessary to define the number of necessary Gauss points for each type of elements as shown in Fig. 5. In general, the elements can be classified into five types such as

i) Tip element is the element containing a crack tip. All nodes belonging to a tip element are enriched with the near-tip fields of Eq. (28).

ii) Split elements are elements that completely cut by the crack. Their nodes are enriched by the discontinuous Heaviside function displayed in Eq. (27).

iii) Tip blending elements are elements which is around tip elements. Some of these elements' nodes are enriched with the near-tip fields and others are not enriched at all.

iv) Split blending elements are elements neighboring split elements. Some of these elements' nodes are enriched with the discontinuous function, and others are not enriched at all.

v) Standard elements are elements that are in none of the above categories. None of their associated nodes are enriched.

In the numerical implementation [74], the tip elements and split elements are first subdivided into 3 or 5 sub-triangles as shown in Fig. 7. Then the number of necessary Gauss points for five types of elements, as shown in Fig. 8, can be defined as below:

· Tip elements: 65 Gauss points for each triangular sub-element.

· Split elements: 3 Gauss points for each triangular sub-element.

· Tip blending elements: 13 Gauss points.

· Split blending elements: 1 Gauss point.

· Standard elements: 1 Gauss point.

4 Numerical results

In this section, a cracked shell with geometry as shown in Fig. 9 with different crack locations is investigated to illustrate the robustness and effectiveness of the XCS-FEM-DSG3 for free vibration of cracked shell analysis. Material parameters of the shell is given by the elastic modulus $E = 2.1 \times 10^{11}(\mathrm{N/m^2})$, Poisson's ratio $\nu = 0.3$ and material mass density $\rho = 7860(\mathrm{kg/m^3})$. For each crack location, free vibration behaviors of the shell are analyzed and compared to that of the commerical software ANSYS in order to confirm the accuracy of XCS-FEM-DSG3. In the analysis performed by the ANSYS, the "shell 63" element is used to model and analyze the problem.

4.1 Free vibration analysis of cylindrical shell with middle crack along *y*-axis

This section investigates the free vibration behavior of a cracked shell possesing middle crack along *y*-axis as shown in Fig. 10 and compares to that of ANSYS sofware to illustrate the robustness of XCS-FEM-DSG3 in free vibration analysis of cracked shell. The shell behavior with different crack lengths is analyzed to further investigate the effect of crack length on shell structures' vibration response.

The results of first five natural frequency values with different values of crack lengths are shown in Table 1. From the table, it can be seen that results by the XCS-FEM-DSG3 agree very well with those by commercial software ANSYS. In fact, all relative errors for cases of crack lengths are less than 5%. It can also be observed from the table that crack length significantly affects free vibration behavior of cracked shell. The natural frequency values decrease largely when crack lengths increase for all vibration modes. This phenomenon is understandable because the presence and propagation of crack cause the decrease of shell's stiffness which results in decrease of natural frequency values. This hence illustrates the robustness and reliability of XCS-FEM-DSG3 for free

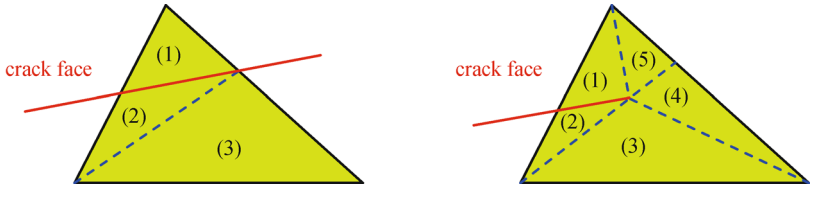

Fig. 7 Illustration of subdividing the Heaviside enriched elements and the crack-tip elements into sub-triangles

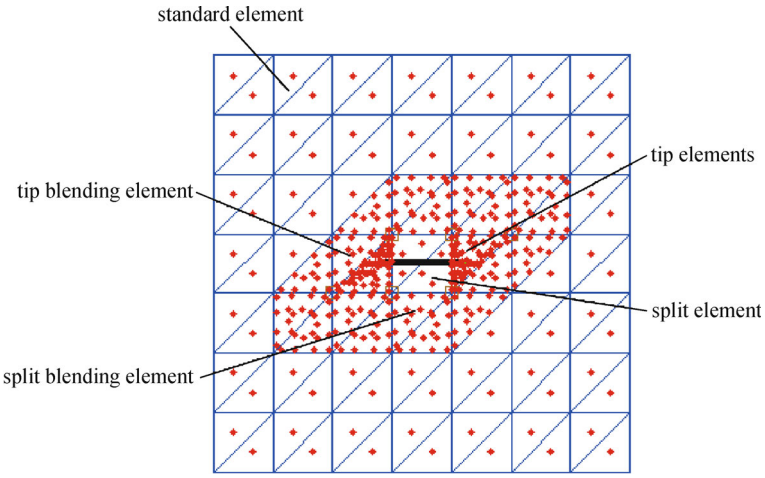

Fig. 8 Gauss quadrature rules for elements: tip elements, split element, tip blending element, split blending element and standard element

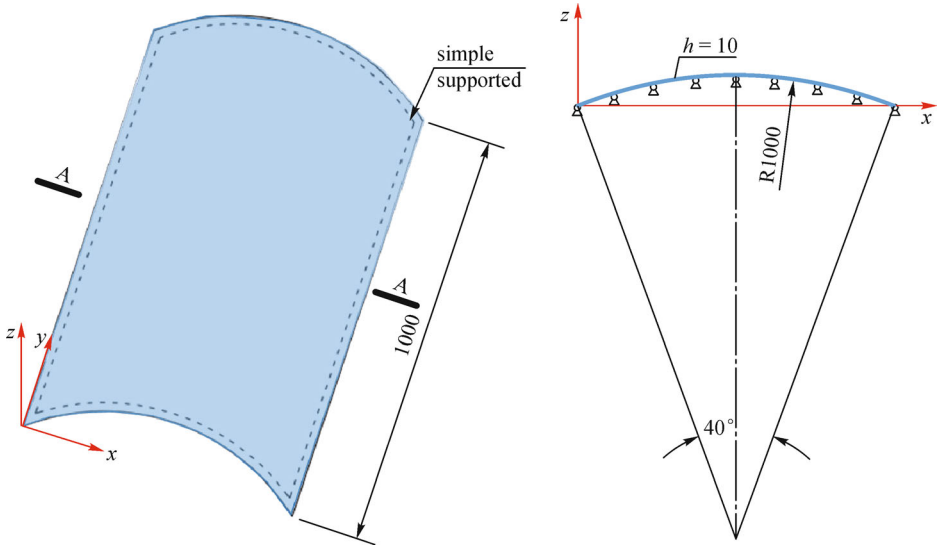

Fig. 9 Simple supported shell model (length unit mm)

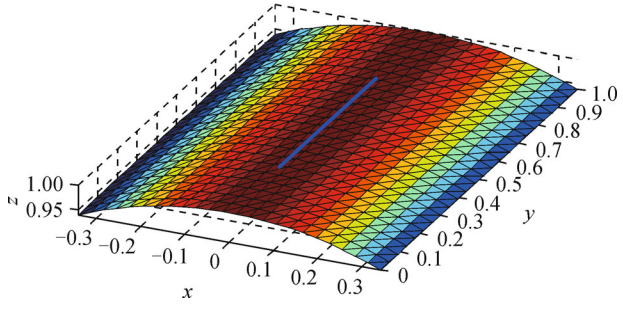

Fig. 10 Finite element model of shell with middle crack along *y*-axis at mesh 24×24

vibration analysis of cracked cylindrical shell.

The results of free vibration analysis with crack length l = 0.3 m at different mesh sizes and crack location are presented in Table 2 to investigate the convergence of XCS-FEM-DSG3. From the table, it can be seen that when the mesh size increases, the natural frequency values decrease in a stable rate. This again illustrates the stability and reliability of XCS-FEM-DSG3. At the same mesh size of 40 × 40, the results by XCS-FEM-DSG3 are pretty worse than that of ANSYS, but the results brought by XCS-FEM-DSG3 are very close to those by ANSYS at the mesh 60 × 60. It is worthy to note that the XCS-FEM-DSG3 uses only low order triangular elements, while ANSYS uses the nine-node quarter-point quadratic element which is a high order quadratic element. As a result, it can be seen that XCS-FEM-DSG3 is a simple and robust method for free vibration analysis of cracked cylindrical shell.

Table 1 First five natural frequency values of shell with middle crack along *y*-axis

crack length/m	methods & comparison	natural frequency values				
		mode 1	mode 2	mode 3	mode 4	mode 5
$l = 0.1$	XCS-FEM-DSG3	249.26	277.92	411.24	488.39	568.60
	ANSYS	244.10	272.54	401.60	474.27	556.95
	relative error/%	**2.07**	**1.94**	**2.34**	**2.89**	**2.05**
$l = 0.2$	XCS-FEM-DSG3	247.85	271.55	406.21	466.53	566.92
	ANSYS	242.37	267.97	396.79	453.44	555.08
	relative error/%	**2.21**	**1.32**	**2.32**	**2.81**	**2.09**
$l = 0.3$	XCS-FEM-DSG3	240.81	253.83	398.18	438.11	556.27
	ANSYS	234.81	246.18	389.12	427.74	543.40
	relative error/%	**2.49**	**3.01**	**2.28**	**2.37**	**2.31**
$l = 0.4$	XCS-FEM-DSG3	221.91	224.20	387.53	414.70	454.11
	ANSYS	215.89	216.56	379.10	406.20	439.79
	relative error/%	**2.71**	**3.41**	**2.18**	**2.05**	**3.15**
$l = 0.5$	XCS-FEM-DSG3	191.08	192.29	373.29	395.25	397.38
	ANSYS	184.26	186.56	365.01	386.79	389.47
	relative error/%	**3.57**	**2.98**	**2.22**	**2.14**	**1.99**

Table 2 Natural frequency values of shell with middle crack along *y*-axis and crack length $l = 0.3$ m

methods & comparison	mesh size	natural frequency values				
		mode 1	mode 2	mode 3	mode 4	mode 5
XCS-FEM-DSG3	24×24	247.32	262.68	405.77	460.88	565.14
	28×28	243.11	254.39	401.37	445.34	557.17
	32×32	240.89	252.51	398.64	438.53	556.82
	40×40	240.81	253.83	398.18	438.11	556.27
	60×60	235.09	249.80	386.56	425.42	540.76
ANSYS	40×40	234.81	246.18	389.12	427.74	543.4

The first three vibration mode shapes of both intact shell and cracked shell with crack length $l = 0.3$ m are presented respectively in Fig. 11 and Fig. 12 in comparison with those by commercial software ANSYS. From the figures, it can be seen that vibration mode shapes are changed considerably with the presence of crack. This shows that the crack has significant impact on cylindrical shell's vibration behavior. As a result, the presence of crack should be taken into account seriously in process of analysis for shell structures. It also can be seen that the free vibration mode shapes by XCS-FEM-DSG3 are closely similar to those by ANSYS in all cases. This further illustrates the suitability and accuracy of XCS-FEM-DSG3 for free vibration analysis of cracked cylindrical shell.

4.2 Free vibration analysis of cylindrical shell with side crack along *y*-axis

Free vibration behavior of the cracked cylindrical shell with side crack along *x*-axis as shown in Fig. 13 is examined. The numerical results are compared with those by ANSYS to illustrate the effectiveness of XCS-FEM-DSG3 in solving free vibration of shell strucutres.

The first five natural frequencies of side cracked shell with different crack lengths are presented in Table 3 in comparison with those by ANSYS. As shown in the table, all relative error values between results by XCS-FEM-DSG3 and those by ANSYS is smaller than 5%. This further illustrates the reliability and accuracy of XCS-FEM-DSG3 in analyzing free vibration behavior of crack shell. In good agreement with the case of middle crack along *y*-axis, the presence and propagation of crack cause the frequency values to decrease significantly. This illustrates the important influence of crack on shell structures' free vibration behavior.

The frequency values of first five vibration modes are presented in Table 4 with crack length 0.3 and different mesh sizes. As seen in the table, the results converge in a stable rate. With the same mesh size, the difference between results by the XCS-FEM-DSG3 and those by

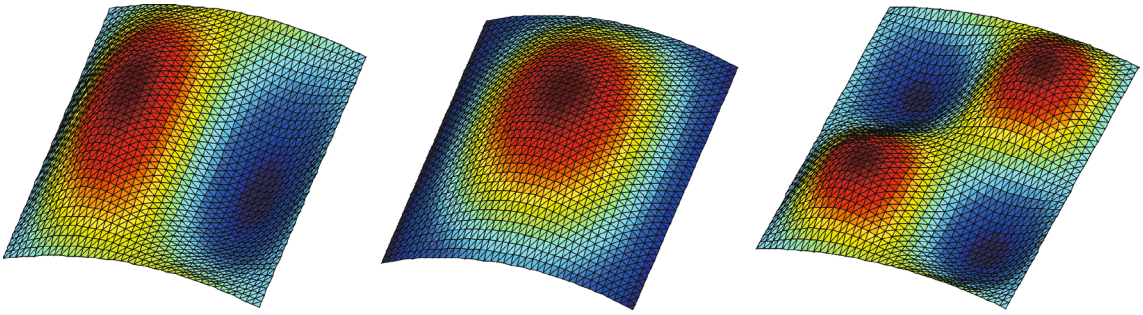

Fig. 11 The first three free vibration mode shapes of the intact cylindrical shell

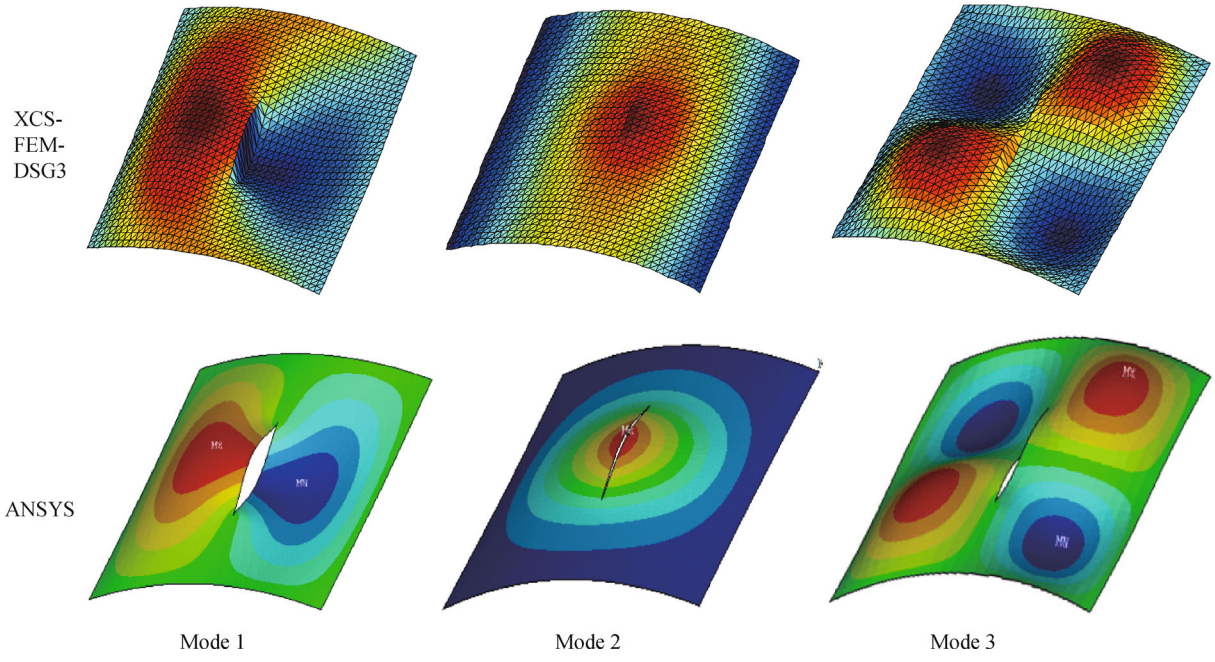

Fig. 12 The first three mode shapes with middle crack along y-axis at crack length $l = 0.3$

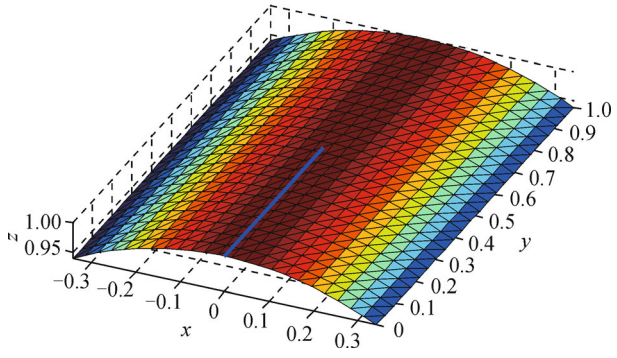

Fig. 13 Finite element model of cracked shell with side crack along y-axis at mesh 24×24 and crack length $l = 0.5$ m

ANSYS are relatively small. In addition, the first three vibration mode shapes are shown in Fig. 14 in comparison to those by ANSYS. It can be seen that the mode shapes are significantly different to mode shapes of the intact structure. This is because the presence of crack at shell's side significantly cause shell stiffness to decrease considerably right at crack location. It is this localized decrease that cause free vibration modes to be asymetric which far different from that of the intact structure. This further confirms the considerable impact of crack on cylindrical shell. As presented in the figure, the mode shapes by XCS-FEM-DSG3 agree well with that of ANSYS. The accuracy and reliability of XCS-FEM-DSG3 in free vibration analysis for cracked cylindrical shell is hence further verified.

4.3 Free vibration analysis of cylindrical shell with middle crack along x-axis

The final numerical example is the cylindrical shell with middle crack along x-axis as shown in Fig. 15. As in two examples presented above, free vibration behavior of the shell is analyzed with various crack length $l = 0.1 \div 0.3$ m

Table 3 First five natural frequency values of shell with side crack along *y*-axis

crack length/m	methods & comparison	natural frequency values				
		mode 1	mode 2	mode 3	mode 4	mode 5
$l = 0.1$	XCS-FEM-DSG3	249.26	279.09	409.57	493.0	567.90
	ANSYS	243.76	273.71	399.53	481.3	555.75
	relative error/%	**2.21**	**1.93**	**2.45**	**2.37**	**2.14**
$l = 0.2$	XCS-FEM-DSG3	247.47	278.34	399.44	490.17	541.51
	ANSYS	242.28	272.79	389.19	477.75	521.17
	relative error/%	**2.10**	**1.99**	**2.57**	**2.53**	**3.76**
$l = 0.3$	XCS-FEM-DSG3	242.41	270.90	376.62	418.65	480.85
	ANSYS	237.07	264.78	365.07	402.18	467.74
	relative error/%	**2.20**	**2.26**	**3.07**	**3.93**	**2.73**
$l = 0.4$	XCS-FEM-DSG3	224.35	239.52	327.81	354.57	452.75
	ANSYS	218.70	231.64	318.68	345.45	440.96
	relative error/%	**2.52**	**3.29**	**2.79**	**2.57**	**2.60**
$l = 0.5$	XCS-FEM-DSG3	190.28	194.66	303.68	344.93	423.02
	ANSYS	183.29	186.01	296.54	338.43	412.55
	relative error/%	**3.67**	**4.44**	**2.35**	**1.88**	**2.48**

Table 4 Natural frequency values of shell with side crack along *y*-axis and crack length $l = 0.3$ m

methods & comparison	mesh size	natural frequency values				
		mode 1	mode 2	mode 3	mode 4	mode 5
XCS-FEM-DSG3	24×24	246.31	274.19	388.88	441.14	493.54
	28×28	243.12	270.44	377.33	418.37	485.06
	32×32	242.78	270.41	377.19	421.77	483.57
	40×40	242.41	270.9	376.62	418.65	480.85
	60×60	241.23	270.11	373.01	413.14	477.12
ANSYS	40×40	237.07	264.78	365.07	402.18	467.74

to further investigate the effect of crack on shell structures.

The first five frequency values are shown in Table 5 compared to that from ANSYS software for different cases of crack length. For this case, almost all the relative errors between XCS-FEM-DSG3 and ANSYS are less than 3%. The difference is understandable because the XCS-FEM-DSG3 used only low order triangular element while ANSYS used nine-node quarter-point quadratic elements. As predicted, the high order elements used by ANSYS would give better results compared to lower order elements. This one more time strengthens the conclusion that XCS-FEM-DSG3 is a simple, robust and appropriate method for free vibration analysis of cracked cylindrical shell.

With different mesh size, the first five frequency values of the XCS-FEM-DSG3 are presented as in Table 6 and compared to that of ANSYS. The stability of XCS-FEM-DSG3 is further proven by the fact that the change rate of natural frequency values through different mesh sizes is stable for all vibration modes. Figure 16 demonstrates the first three mode shapes of cylindrical shell with crack length $l = 0.3$ m compared with that of ANSYS. It can be seen that the mode shapes with presence of crack along *x*-axis are slightly different to that of intact structures. However, the difference is still considerable, especially for mode 1. This shows that middle crack along *x*-axis might has less impact on free vibration behavior of cylindrical shell than middle and side crack along *y*-axis. The good agreement in mode shapes between XCS-FEM-DSG3 and ANSYS in Fig. 16 illustrates the accuracy and reliability of XCS-FEM-DSG3 for free vibration analysis of cracked cylindrical shell.

5 Conclusion

In the paper, the XFEM is integrated into the CS-FEM-DSG3 to give a so-called XCS-FEM-DSG3 for free

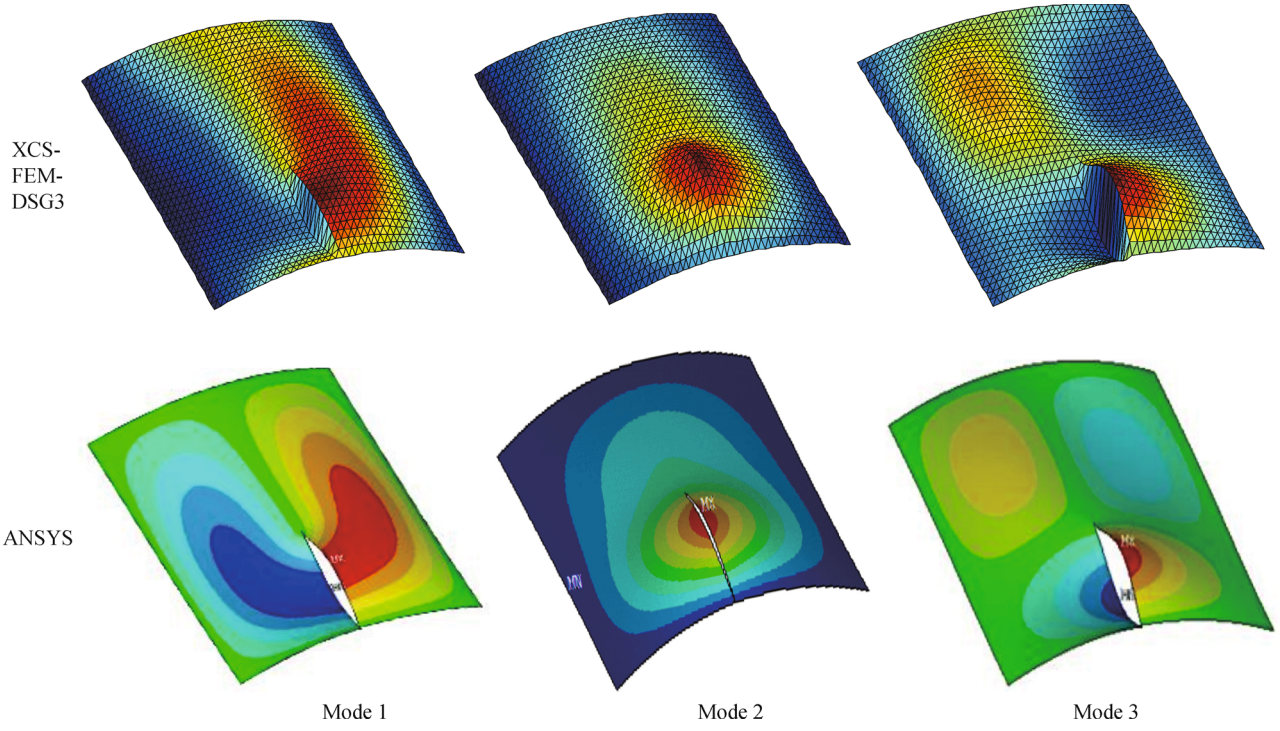

Fig. 14 The first three mode shapes with middle side along y-axis at crack lengths l = 0.3 m

Table 5 First five natural frequency values of shell with middle crack along x-axis

crack length/m	methods & comparison	natural frequency values				
		mode 1	mode 2	mode 3	mode 4	mode 5
l = 0.1	XCS-FEM-DSG3	250.06	275.03	412.17	494.88	569.96
	ANSYS	244.71	269.96	405.08	480.69	554.18
	relative error/%	**2.14**	**1.84**	**1.72**	**2.87**	**2.77**
l = 0.2	XCS-FEM-DSG3	249.57	258.09	406.18	492.72	567.84
	ANSYS	244.69	252.92	403.48	479.71	546.33
	relative error/%	**1.95**	**2.01**	**0.66**	**2.64**	**3.79**
l = 0.3	XCS-FEM-DSG3	226.39	244.07	388.47	486.68	550.08
	ANSYS	221.99	242.21	393.48	479.46	533.76
	relative error/%	**1.94**	**0.76**	**1.29**	**1.48**	**2.97**

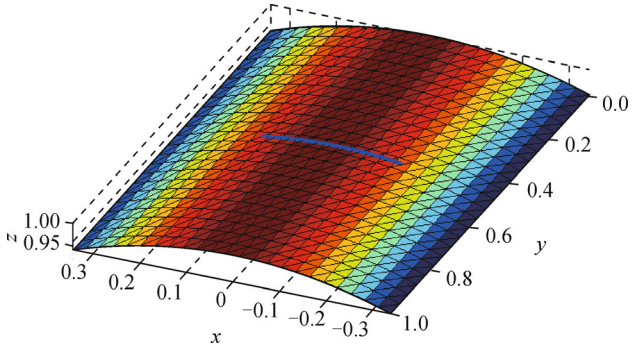

Fig. 15 Finite element model of cracked shell with middle crack along x-axis at mesh 24×24 and crack length l = 0.3 m

vibration analysis of cracked cylindrical shell structures. In the process of analysis, the stiffness matrix of uncut elements is formulated by the conventional CS-FEM-DSG3, while stiffness matrix of elements cut by crack is calculated by the XCS-FEM-DSG. In the formulation of XCS-FEM-DSG3, the discontinuity and localization of crack in shell structures are formulated by enrichment functions. Three numerical example of free vibration analysis of cracked cylindrical shell with different crack locations and crack lengths are solved and compared with the commercial software ANSYS to illustrate the accuracy and reliability of XCS-FEM-DSG3. The numerical results show that the XCS-FEM-DSG3 is a simple, robust and

Table 6 Natural frequency values of shell with middle crack along *x*-axis and crack length $l = 0.3$ m

methods & comparison	mesh size	natural frequency values				
		mode 1	mode 2	mode 3	mode 4	mode 5
XCS-FEM-DSG3	24×24	235.54	249.45	402.87	497.5	561.29
	28×28	231.35	248.03	398.56	494.06	557.22
	32×32	227.12	247.00	395.46	491.94	553.32
	40×40	226.39	244.07	388.47	486.68	550.08
	60×60	224.18	241.87	384.51	482.95	546.28
ANSYS	40×40	221.99	242.21	393.48	479.46	553.76

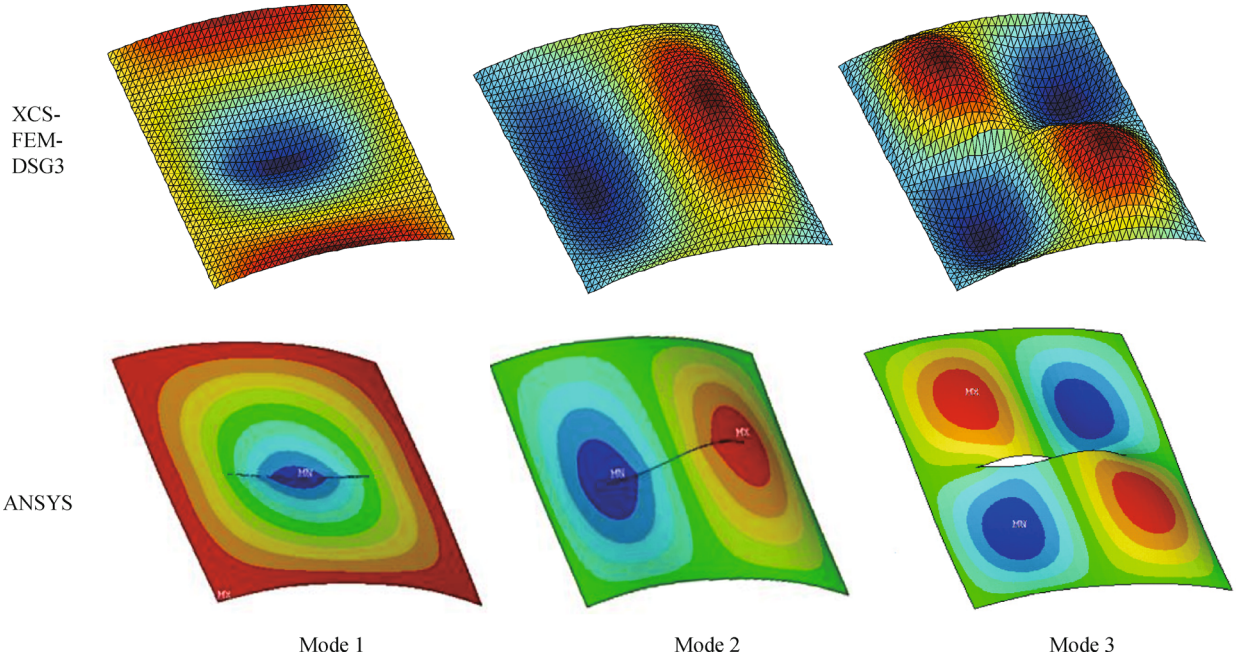

Fig. 16 The first three mode shapes with middle crack along *x*-axis at crack length $l = 0.3$ m

appropriate method for free vibration analysis of cracked Reissner-Mindlin cylindrical shells.

In general, the novel method possesses three main advantages including: (i) the mesh is generated independent of cracks which helps avoid remeshing as in conventional FEM; (ii) the presence of CS-FEM-DSG3 in analyzing the cylindrical shell's behaviors helps overcome the shearlocking phenomenon and improve the accuracy of solutions considerably. This is due to softening effect of the cell-based strain smoothing technique; and (iii) the method is very flexible to apply for arbitrary complicated geometric domains due to using only three-node triangular elements which can be easily generated automatically.

Acknowledgements This research is funded by Foundation for Science and Technology Development of Ton Duc Thang University (FOSTECT), website: http://fostect.tdt.edu.vn, under Grant No. FOSTECT.2014.BR.01.

References

1. Kwon Y W. Development of finite element shape functions with derivative singularity. Computers & Structures, 1988, 30(5): 1159–1163
2. Krawczuk M. Rectangular shell finite element with an open crack. Finite Elements in Analysis and Design, 1994, 15(3): 233–253
3. Liu R, Zhang T, Wu X, Wang C. Determination of stress intensity factors for a cracked shell under bending with improved shell theories. Journal of Aerospace Engineering, 2006, 19(1): 21–28
4. Vaziri A, Estekanchi H E. Buckling of cracked cylindrical thin shells under combined internal pressure and axial compression. Thin-walled Structures, 2006, 44(2): 141–151
5. Fu J, To C W S. Bulging factors and geometrically nonlinear responses of cracked shell structures under internal pressure. Engineering Structures, 2012, 41: 456–463
6. Belytschko T, Black T. Elastic crack growth in finite elements with minimal remeshing. International Journal for Numerical Methods in

Engineering, 1999, 45(5): 601–620
7. Moës N, Dolbow J, Belytschko T. A finite element method for crack growth without remeshing. International Journal for Numerical Methods in Engineering, 1999, 46: 131–150
8. Stolarska M, Chopp D L, Moës N, Belytschko T. Modelling crack growth by level sets in the extended finite element method. International Journal for Numerical Methods in Engineering, 2001, 51(8): 943–960
9. Bachene M, Tiberkak R, Rechak S. Vibration analysis of cracked plates using the extended finite element method. Archive of Applied Mechanics, 2009, 79(3): 249–262
10. Natarajan S, Baiz P M, Bordas S, Rabczuk T, Kerfriden P. Natural frequencies of cracked functionally graded material plates by the extended finite element method. Composite Structures, 2011, 93 (11): 3082–3092
11. Rabczuk T, Areias P M A. A meshfree thin shell for arbitrary evolving cracks based on an external enrichment. CMES-Computer Modeling in Engineering and Sciences, 2006, 16: 115–130
12. Rabczuk T, Areias P M A, Belytschko T. A meshfree thin shell method for non-linear dynamic fracture. International Journal for Numerical Methods in Engineering, 2007, 72(5): 524–548
13. Zhuang X, Augarde C E, Mathisen K M. Fracture modeling using meshless methods and level sets in 3D: Framework and modeling. International Journal for Numerical Methods in Engineering, 2012, 92(11): 969–998
14. Chau-Dinh T, Zi G, Lee P S, Rabczuk T, Song J H. Phantom-node method for shell models with arbitrary cracks. Computers & Structures, 2012, 92–93: 242–256
15. Ghorashi S S, Valizadeh N, Mohammadi S, Rabczuk T. T-spline based XIGA for fracture analysis of orthotropic media. Computers & Structures, 2015, 147: 138–146
16. Nguyen-Thanh N, Valizadeh N, Nguyen M N, Nguyen-Xuan H, Zhuang X, Areias P, Zi G, Bazilevs Y, De Lorenzis L, Rabczuk T. An extended isogeometric thin shell analysis based on Kirchhoff–Love theory. Computer Methods in Applied Mechanics and Engineering, 2015, 284: 265–291
17. Areias P, Rabczuk T. Finite strain fracture of plates and shells with configurational forces and edge rotations. International Journal for Numerical Methods in Engineering, 2013, 94(12): 1099–1122
18. Areias P, Rabczuk T, Camanho P P. Initially rigid cohesive laws and fracture based on edge rotations. Computational Mechanics, 2013, 52(4): 931–947
19. Areias P, Rabczuk T, Dias-da-Costa D. Element-wise fracture algorithm based on rotation of edges. Engineering Fracture Mechanics, 2013, 110: 113–137
20. Areias P, Rabczuk T, Camanho P P. Finite strain fracture of 2D problems with injected anisotropic softening elements. Theoretical and Applied Fracture Mechanics, 2014, 72: 50–63
21. Liu G R, Nguyen-Thoi T. Smoothed Finite Element Methods. NewYork: Taylor and Francis Group, 2010
22. Liu G R, Nguyen-Thoi T, Nguyen-Xuan H, Dai K Y, Lam K Y. On the essence and the evaluation of the shape functions for the smoothed finite element method (SFEM). International Journal for Numerical Methods in Engineering, 2009, 77(13): 1863–1869
23. Nguyen T T, Liu G R, Dai K Y, Lam K Y. Selective smoothed finite element method. Tsinghua Science and Technology, 2007, 12(5): 497–508
24. Liu G R, Dai K Y, Nguyen T T. A smoothed finite element method for mechanics problems. Computational Mechanics, 2007, 39(6): 859–877
25. Nguyen-Thoi T, Liu G R, Nguyen-Xuan H. Additional properties of the node-based smoothed finite element method (NS-FEM) for solid mechanics problems. International Journal of Computational Methods, 2009, 06(04): 633–666
26. Nguyen-Thoi T, Liu G R, Nguyen-Xuan H, Nguyen-Tran C. Adaptive analysis using the node-based smoothed finite element method (NS-FEM). International Journal for Numerical Methods in Biomedical Engineering, 2011, 27(2): 198–218
27. Liu G R, Nguyen-Thoi T, Nguyen-Xuan H, Lam K Y. A node-based smoothed finite element method (NS-FEM) for upper bound solutions to solid mechanics problems. Computers & Structures, 2009, 87(1–2): 14–26
28. Nguyen-Thoi T, Liu G R, Nguyen-Xuan H, Nguyen-Tran C. An n-sided polygonal edge-based smoothed finite element method (nES-FEM) for solid mechanics. International Journal for Numerical Methods in Biomedical Engineering, 2011, 27: 1446–1472
29. Liu G R, Nguyen-Thoi T, Lam K Y. An edge-based smoothed finite element method (ES-FEM) for static, free and forced vibration analyses of solids. Journal of Sound and Vibration, 2009, 320(4–5): 1100–1130
30. Nguyen-Thoi T, Liu G R, Lam K Y, Zhang G Y. A face-based smoothed finite element method (FS-FEM) for 3D linear and geometrically non-linear solid mechanics problems using 4-node tetrahedral elements. International Journal for Numerical Methods in Engineering, 2009, 78(3): 324–353
31. Liu G R, Nguyen-Xuan H, Nguyen-Thoi T, Xu X. A novel Galerkin-like weakform and a superconvergent alpha finite element method (S-alpha FEM) for mechanics problems using triangular meshes. Journal of Computational Physics, 2009, 228(11): 4055–4087
32. Liu G R, Nguyen-Thoi T, Lam K Y. A novel alpha finite element method (αFEM) for exact solution to mechanics problems using triangular and tetrahedral elements. Computer Methods in Applied Mechanics and Engineering, 2008, 197(45–48): 3883–3897
33. Liu G R, Nguyen-Xuan H, Nguyen-Thoi T. A variationally consistent alpha FEM (VC alpha FEM) for solution bounds and nearly exact solution to solid mechanics problems using quadrilateral elements. International Journal for Numerical Methods in Engineering, 2011, 85(4): 461–497
34. Liu G R, Nguyen-Thoi T, Lam K Y. A novel FEM by scaling the gradient of strains with factor alpha (alpha FEM). Computational Mechanics, 2009, 43(3): 369–391
35. Liu G R, Nguyen T T, Dai K Y, Lam K Y. Theoretical aspects of the smoothed finite element method (SFEM). International Journal for Numerical Methods in Engineering, 2007, 71(8): 902–930
36. Liu G R, Nguyen-Xuan H, Nguyen-Thoi T. A theoretical study on the smoothed FEM (S-FEM) models: Properties, accuracy and convergence rates. International Journal for Numerical Methods in Engineering, 2010, 84(10): 1222–1256
37. Nguyen-Xuan H, Rabczuk T, Bordas S, Debongnie J F. A smoothed finite element method for plate analysis. Computer Methods in Applied Mechanics and Engineering, 2008, 197(13–16): 1184–1203

38. Nguyen-Xuan H, Liu G R, Thai-Hoang C, Nguyen-Thoi T. An edge-based smoothed finite element method (ES-FEM) with stabilized discrete shear gap technique for analysis of Reissner–Mindlin plates. Computer Methods in Applied Mechanics and Engineering, 2010, 199(9–12): 471–489
39. Nguyen-Xuan H, Rabczuk T, Nguyen-Thanh N, Nguyen-Thoi T, Bordas S. A node-based smoothed finite element method with stabilized discrete shear gap technique for analysis of Reissner–Mindlin plates. Computational Mechanics, 2010, 46(5): 679–701
40. Nguyen-Xuan H, Tran L V, Nguyen-Thoi T, Vu-Do H C. Analysis of functionally graded plates using an edge-based smoothed finite element method. Composite Structures, 2011, 93(11): 3019–3039
41. Nguyen-Xuan H, Tran L V, Thai C H, Nguyen-Thoi T. Analysis of functionally graded plates by an efficient finite element method with node-based strain smoothing. Thin-walled Structures, 2012, 54: 1–18
42. Thai C H, Tran L V, Tran D T, Nguyen-Thoi T, Nguyen-Xuan H. Analysis of laminated composite plates using higher-order shear deformation plate theory and node-based smoothed discrete shear gap method. Applied Mathematical Modelling, 2012, 36(11): 5657–5677
43. Nguyen-Thoi T, Bui-Xuan T, Phung-Van P, Nguyen-Xuan H, Ngo-Thanh P. Static, free vibration and buckling analyses of stiffened plates by CS-FEM-DSG3 using triangular elements. Computers & Structures, 2013, 125: 100–113
44. Nguyen-Thoi T, Phung-Van P, Luong-Van H, Nguyen-Van H, Nguyen-Xuan H. A cell-based smoothed three-node Mindlin plate element (CS-MIN3) for static and free vibration analyses of plates. Computational Mechanics, 2013, 51(1): 65–81
45. Nguyen-Thoi T, Phung-Van P, Thai-Hoang C, Nguyen-Xuan H. A cell-based smoothed discrete shear gap method (CS-DSG3) using triangular elements for static and free vibration analyses of shell structures. International Journal of Mechanical Sciences, 2013, 74: 32–45
46. Phan-Dao H H, Nguyen-Xuan H, Thai-Hoang C, Nguyen-Thoi T, Rabczuk T. An edge-based smoothed finite element method for analysis of laminated composite plates. International Journal of Computational Methods, 2013, 10(01): 1340005
47. Phung-Van P, Nguyen-Thoi T, Tran L V, Nguyen-Xuan H. A cell-based smoothed discrete shear gap method (CS-DSG3) based on the C0-type higher-order shear deformation theory for static and free vibration analyses of functionally graded plates. Computational Materials Science, 2013, 79: 857–872
48. Luong-Van H, Nguyen-Thoi T, Liu G R, Phung-Van P. A cell-based smoothed finite element method using three-node shear-locking free Mindlin plate element (CS-FEM-MIN3) for dynamic response of laminated composite plates on viscoelastic foundation. Engineering Analysis with Boundary Elements, 2014, 42: 8–19
49. Nguyen-Thoi T, Bui-Xuan T, Phung-Van P, Nguyen-Hoang S, Nguyen-Xuan H. An edge-based smoothed three-node mindlin plate element (ES-MIN3) for static and free vibration analyses of plates. KSCE Journal of Civil Engineering, 2014, 18(4): 1072–1082
50. Phung-Van P, Nguyen-Thoi T, Luong-Van H, Lieu-Xuan Q. Geometrically nonlinear analysis of functionally graded plates using a cell-based smoothed three-node plate element (CS-MIN3) based on the C0-HSDT. Computer Methods in Applied Mechanics and Engineering, 2014, 270: 15–36
51. Phung-Van P, Nguyen-Thoi T, Le-Dinh T, Nguyen-Xuan H. Static and free vibration analyses and dynamic control of composite plates integrated with piezoelectric sensors and actuators by the cell-based smoothed discrete shear gap method (CS-FEM-DSG3). Smart Materials and Structures, 2013, 22(9): 17
52. Nguyen-Xuan H, Liu G R, Nguyen-Thoi T, Nguyen-Tran C. An edge-based smoothed finite element method for analysis of two-dimensional piezoelectric structures. Smart Materials and Structures, 2009, 18(6): 1–12
53. Liu G R, Chen L, Nguyen-Thoi T, Zeng K Y, Zhang G Y. A novel singular node-based smoothed finite element method (NS-FEM) for upper bound solutions of fracture problems. International Journal for Numerical Methods in Engineering, 2010, 83(11): 1466–1497
54. Nguyen-Thoi T, Liu G R, Vu-Do H C, Nguyen-Xuan H. A face-based smoothed finite element method (FS-FEM) for visco-elastoplastic analyses of 3D solids using tetrahedral mesh. Computer Methods in Applied Mechanics and Engineering, 2009, 198(41–44): 3479–3498
55. Nguyen-Thoi T, Vu-Do H C, Rabczuk T, Nguyen-Xuan H. A node-based smoothed finite element method (NS-FEM) for upper bound solution to visco-elastoplastic analyses of solids using triangular and tetrahedral meshes. Computer Methods in Applied Mechanics and Engineering, 2010, 199(45–48): 3005–3027
56. Nguyen-Thoi T, Liu G R, Vu-Do H C, Nguyen-Xuan H. An edge-based smoothed finite element method for visco-elastoplastic analyses of 2D solids using triangular mesh. Computational Mechanics, 2009, 45(1): 23–44
57. Nguyen-Xuan H, Rabczuk T, Nguyen-Thoi T, Tran T N, Nguyen-Thanh N. Computation of limit and shakedown loads using a node-based smoothed finite element method. International Journal for Numerical Methods in Engineering, 2012, 90(3): 287–310
58. Tran T N, Liu G R, Nguyen-Xuan H, Nguyen-Thoi T. An edge-based smoothed finite element method for primal–dual shakedown analysis of structures. International Journal for Numerical Methods in Engineering, 2010, 82: 917–938
59. Nguyen-Thoi T, Phung-Van P, Rabczuk T, Nguyen-Xuan H, Le-Van C. An application of the ES-FEM in solid domain for dynamic analysis of 2d fluid-solid interaction problems. International Journal of Computational Methods, 2013, 10
60. Nguyen-Thoi T, Phung-Van P, Rabczuk T, Nguyen-Xuan H, Le-Van C. Free and forced vibration analysis using the n-sided polygonal Cell-Based Smoothed Finite Element Method (NCS-FEM). International Journal of Computational Methods, 2013, 10 (01): 1340008
61. Bletzinger K U, Bischoff M, Ramm E. A unified approach for shear-locking-free triangular and rectangular shell finite elements. Computers & Structures, 2000, 75(3): 321–334
62. Phung-Van P, Nguyen-Thoi T, Tran L V, Nguyen-Xuan H. A cell-based smoothed discrete shear gap method (CS-DSG3) based on the C-0-type higher-order shear deformation theory for static and free vibration analyses of functionally graded plates. Computational Materials Science, 2013, 79: 857–872
63. Phung-Van P, Nguyen-Thoi T, Dang-Trung H, Nguyen-Minh N. A cell-based smoothed discrete shear gap method (CS-FEM-DSG3) using layerwise theory based on the C0-type higher-order shear

deformation for static and free vibration analyses of sandwich and composite plates. Composite Structures, 2014, 111: 553–565

64. Phung-Van P, Luong-Van H, Nguyen-Thoi T, Nguyen-Xuan H. A cell-based smoothed discrete shear gap method (CS-DSG3) based on the higher-order shear deformation theory for dynamic responses of Mindlin plates on the viscoelastic foundation subjected to a moving sprung vehicle. International Journal for Numerical Methods in Engineering, 2014, 98(13): 988–1014
65. Phung-Van P, Nguyen-Thoi T, Luong-Van H, Thai-Hoang C, Nguyen-Xuan H. A cell-based smoothed discrete shear gap method (CS-FEM-DSG3) using layerwise deformation theory for dynamic response of composite plates resting on viscoelastic foundation. Computer Methods in Applied Mechanics and Engineering, 2014, 272: 138–159
66. Bischoff M, Bletzinger K U. Stabilized DSG plate and shell elements. Trends in Computational structural mechanics. CIMNE. Barcelona, Spain, 2001
67. Lyly M, Stenberg R, Vihinen T. A stable bilinear element for the Reissner-Mindlin plate model. Computer Methods in Applied Mechanics and Engineering, 1993, 110(3–4): 343–357
68. Babuška I, Caloz G, Osborn J. Special finite element methods for a class of second order elliptic problems with rough coefficients. SIAM Journal on Numerical Analysis, 1994, 31(4): 945–981
69. Melenk J M. On Generalized Finite Element Methods. University of Maryland, 1995
70. Babuška I, Melenk J. The partition of unity finite element method. International Journal for Numerical Methods in Engineering, 1997, 40(4): 727–758
71. Simone A, Duarte C A, Van der Giessen E. A Generalized Finite Element Method for polycrystals with discontinuous grain boundaries. International Journal for Numerical Methods in Engineering, 2006, 67(8): 1122–1145
72. Babuška I, Nistor V, Tarfulea N. Generalized finite element method for second-order elliptic operators with Dirichlet boundary conditions. Journal of Computational and Applied Mathematics, 2008, 218(1): 175–183
73. Dolbow J, Moës N, Belytschko T. Modeling fracture in Mindlin–Reissner plates with the extended finite element method. International Journal of Solids and Structures, 2000, 37(48–50): 7161–7183
74. Ventura G. On the elimination of quadrature subcells for discontinuous functions in the eXtended Finite-Element Method. International Journal for Numerical Methods in Engineering, 2006, 66(5): 761–795